Lattice strain and static disorder determination in $Si/Si_{1-x}Ge_x/Si$ heterostructures by convergent beam electron diffraction

Stefano Frabboni* and Francesca Gambetta
Istituto Nazionale Fisica della Materia (INFM) and Dipartimento di Fisica, Università di Modena e Reggio Emilia, Via G. Campi 213/A, 41100 Modena, Italy

Aldo Armigliato, Roberto Balboni, Simone Balboni, and Franco Cembali
CNR-Istituto LAMEL, Via P. Gobetti 101, 40129 Bologna, Italy
(Received 14 May 1999)

Lattice strain and static disorder present in $Si_{1-x}Ge_x$ alloys forming $Si/Si_{1-x}Ge_x/Si$ heterostructures with a Ge atomic fraction x equal to 0.1, 0.2, and 0.3, have been studied by convergent beam electron diffraction and large-angle convergent beam electron diffraction. These techniques have been used in order to perform structural analysis of the alloys with a spatial resolution comparable with the dimensions involved in Si/SiGe applications. Strain values along directions both perpendicular and parallel to the sample surface have been determined from a single high-order Laue zone deficiency lines pattern. The resulting relaxed alloy lattice constant has been found to depend on the Ge atomic fraction following a nearest-neighbor model alloy, where the Si-Si, Ge-Ge, and Si-Ge bond lengths combine themselves with a negligible dependence on the Ge atomic fraction. From lattice strain values, both the strain-induced bond bend in the plane of the interface, and the strain-induced bond stretch have been determined. Static disorder measurements, performed by comparing the integrated intensity of high-angle diffracted beams in the silicon substrate and in the SiGe layers, allow the determination of the atomic mean-square displacements produced by the presence in the same coordination shell of Si-Si, Ge-Ge, and Si-Ge atomic pairs with different bond lengths. The measured atomic displacements are greater than the ones predicted by both the nearest-neighbor solution model (which only accounts for the different bond lengths, and not for both bond bend and strain) and a relaxed alloys structure Monte Carlo simulation (which accounts for differences in bond lengths and bond bend, but neglects the effect of strain). The component of the atomic displacement related to the macroscopic strain has been determined as the difference between the experimental values and those computed by Monte Carlo code. A linear correlation between the strain-induced atomic displacement and the strain-induced bond bend in the plane of the interface has been found. [S0163-1829(99)04343-X]

I. INTRODUCTION

Recently much interest has been devoted to Si-based heteroepitaxy from both a fundamental and application point of view. In particular, the SiGe/Si system has been thoroughly investigated[1] because SiGe has opened interesting perspectives in the area of Si-based high-performance devices.[2] Strained SiGe layers form the base of heterojunction bipolar transistors (HBT's) which are currently used in commercial high-speed analog applications. SiGe-based quantum wells have also been the subject of extensive luminescence studies because the energy gap can be adjusted to the 1.3–1.6-μm range by varying the Ge content and the well width. All these applications need a very thin layer of crystalline alloy (thickness ranging from few monolayers to tens of nanometers), free of extended defects, grown between a silicon substrate and a silicon cap. It is then evident that, for a deep comprehension of the physical-chemical properties of the alloys involved in Si/SiGe based devices, a structural characterization with high spatial resolution is necessary.

One of the most important structural parameters to be investigated in the SiGe/Si system is the lattice strain produced in the SiGe film by the coherency constraint imposed by the Si substrate in the plane of the interface. Indeed the band gap of the SiGe alloy, and then its electronic properties, depend on the strain level present in the layers.[1] It is known that the layer, when grown on the Si substrate, is tetragonally strained in an attempt to conserve its unit-cell volume. This distortion is usually described in the frame of the macroscopic-elasticity theory. For an isotropic cubic layer of lattice constant a_R, grown on a (001) Si substrate, the strain in the plane of the interface, $\varepsilon_{\parallel}=(a_{\parallel}-a_R)/a_R$, is related to the one along the direction perpendicular to the interface, $\varepsilon_{\perp}=(a_{\perp}-a_R)/a_R$, through elastic constants of the material $\varepsilon_{\perp}=-[2\nu/(1-\nu)]\varepsilon_{\parallel}$. Here ν is the Poisson coefficient and $a_{\parallel}=a_{Si}$ if the layer is coherent with the substrate. Literature exists on the structural studies of both the strained[3] and relaxed SiGe alloys.[4]

The local atomic arrangement in the alloy (strained and relaxed) has been studied with the extended x-ray-absorption fine-structure (EXAFS) technique. Some authors report that the Si-Si, Ge-Ge, and Si-Ge bond lengths tend to remain close to their natural value in both the relaxed[5] and strained[6] alloys for each Ge content. Aldrich, Nemanich, and Sayers[7] found that the Si-Si, Ge-Ge, and Si-Ge bonds maintain distinctly different lengths, which change linearly with the alloy composition. In any case, in addition to the macroscopical strain, small local (microscopical) distortions in the crystalline lattice exist because of the presence in the same coordi-

nation shell of Si-Si, Ge-Ge, and Si-Ge pairs that have different interatomic distances (static disorder).

The correlation between the macroscopic strain in the planes parallel to the interface and the microscopic structure of the alloy seems an important structural parameter for comprehension of the physical-chemical properties of the material. An experimental study of this correlation has been reported by Woicik *et al.*[8] using polarization-dependent EXAFS measurements. In that experiment it was found that the first-neighbor bond length only slightly deviates from its unstrained values whereas the distortion of the cubic unit cell produced by strain leads to measurable polarization-dependent changes in the first-shell coordination number and second-shell distances. It was thus suggested that changes in the tetrahedral angle in the planes both parallel and perpendicular to the interface should be present. In particular, the change in the tetrahedral angle in the planes parallel to the interface being roughly two times the one in planes perpendicular to the interface.

All the previously reported structural characterizations are very accurate but suffer from a poor spatial resolution. Techniques like convergent beam electron diffraction (CBED) and large-angle convergent beam electron diffraction (LACBED),[9] available in any analytical transmission electron microscope (TEM) and characterized by nanometric spatial resolution, seem good candidates for the structural characterization of very thin films of alloy. Indeed both the macroscopic strain and the microscopic static disorder produce effects on high-angle electron-diffracted beams excited in CBED and LACBED patterns. In particular, strain causes angular shifts of high-angle diffracted beam,[10] whereas static disorder reduces the coherent Bragg diffracted intensity.[11]

The aim of this paper is to exploit the capabilities of high spatial resolution techniques like CBED and LACBED to the measurement of the *macroscopic* lattice strain and the *microscopic* static disorder present in the alloy forming $Si(20\,nm)Si_{1-x}Ge_x/Si$ heterostructures with Ge atomic content, $x=0.1$, 0.2, and 0.3. The measured strain values, expressed in term of bond bend and bond stretch in a way similar to the one proposed by Woicik *et al.*,[8] will be related to the static disorder data in order to find a correlation between the macroscopic lattice strain and the microscopic arrangement of atoms in the unit cells of the SiGe alloys.

II. EXPERIMENTAL PROCEDURE

A. Sample preparation

The $Si/Si_{1-x}Ge_x/Si$ heterostructures have been deposited by chemical vapor deposition (CVD) on ⟨001⟩ silicon wafers. After removing the native oxide, an $\cong 1$ μm Si buffer layer has been grown at 1050 °C, followed by the growth of a 20-nm-thick $Si_{1-x}Ge_x$ film and of a 120-nm-thick Si cap, both at 700 °C. The atomic fraction of Ge, *x*, was determined in thicker $Si_{1-x}Ge_x$ films, grown in identical conditions for longer times by Rutherford backscattering spectrometry (RBS), which yielded, for the three investigated concentrations, a value $x=0.10\pm0.01$, $x=0.20\pm0.01$, and $x=0.31\pm0.01$. These concentrations were checked by energy dispersion x-ray (EDX) microanalysis on TEM samples. In addition, plan-view measurements indicate that the $Si_{1-x}Ge_x$ layer is fully strained and without defects.

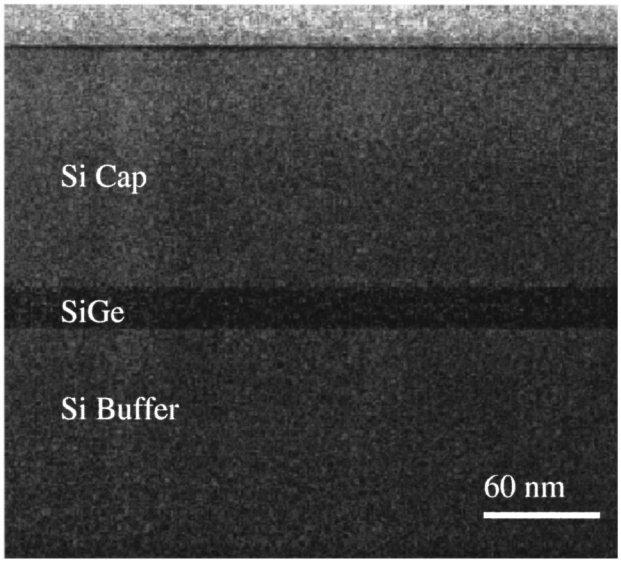

FIG. 1. Cross-sectional bright field TEM image of the $Si/Si_{0.8}Ge_{0.2}$/sample. The $Si/Si_{0.8}Ge_{0.2}/Si$ interfaces appear sharp and without defects.

Preparation of TEM cross sections for strain and static disorder determination involved glueing, sawing, and mechanical lapping down to 20 μm, and low-angle ion beam milling to perforation.

In Fig. 1 a cross-section TEM bright field image of the $Si_{0.8}Ge_{0.2}$ sample is reported. The interfaces appear sharp and free from dislocations. The same morphology has been observed in all the investigated samples so we assume complete pseudomorphic growth for all the three investigated concentrations.

B. Electron-diffraction measurements

A Philips CM30 (S)TEM, equipped with a Gatan MSC 794 1-in. slow-scan change-coupled device (CCD) (SSCCD) camera and operating at 100 kV has been employed for the CBED strain measurements. The ⟨130⟩ zone axis has been selected in order to minimize the dynamical effects on the position of high-order Laue zone deficiency (HOLZ) lines in the central disk of the pattern.[10] The sample temperature has been kept at about 100 K, by using a Gatan liquid nitrogen cooled double-tilting holder, in order to reduce both the thermal diffuse scattering, thus improving the HOLZ-lines visibility, and the contamination. A Philips EM400 operating at 100 kV has been used for LACBED analysis. The patterns have been obtained using a selected area aperture of 5 μm and digitally recorded by means of a Gatan 694 1-in. SSCCD camera. In both cases the microscopes were operating in nanoprobe mode and the incident electron beam was focused to obtain a disk of minimum confusion of about 10 nm [full width at half maximum (FWHM)] in the object plane.

C. CBED strain determination

The in-plane $\varepsilon_{\parallel}=(a_{\parallel}-a_R)/a_R$ and perpendicular $\varepsilon_{\perp}=(a_{\perp}-a_R)/a_R$ strains can be determined if the $a_{\parallel}$, $a_{\perp}$, and a_R lattice parameters are measured. The most accurate electron diffraction method for the measurement of localized lat-

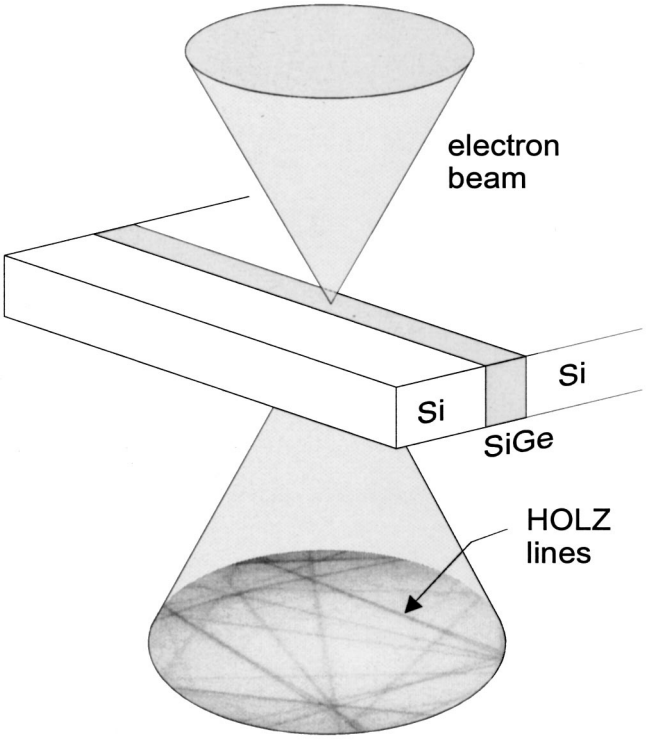

FIG. 2. Experimental geometry used in CBED strain measurements. An electron beam is focused on the sample oriented along a ⟨130⟩ zone axis. HOLZ deficiency lines are formed inside the transmitted disk of the diffraction pattern. The relative position of these lines depends on the lattice parameters (strain).

tice parameters is the HOLZ line method.[10] This method is based on the high sensitivity of the HOLZ lines present in the central disk of the CBED pattern to the variations of the lattice parameters. In Fig. 2 a sketch of the experimental geometry used in this experiment is reported. The samples have been oriented along the ⟨130⟩ zone axis and the HOLZ-line patterns taken in both the silicon substrate and the $Si_{1-x}Ge_x$ film in the middle of the layer. Unwanted relaxation-induced shear strain effects mainly present at the interfaces[12] are thus minimized. The lattice parameter measurements are generally done by fitting the experimental HOLZ-line pattern with simulations having the lattice constants as fitting parameters. A χ^2 criteria similar to that proposed by Zuo[13] has been applied to obtain the best match between the experimental and the simulated diffraction patterns, within the experimental errors determined by the HOLZ-lines width, minimizing the following parameter:

$$\chi^2=\frac{1}{N-m}\sum_{i=1}^{N}\left(\frac{d_i^{\mathrm{expt}}-d_i^{\mathrm{theor}}}{\sigma_i}\right)^2, \qquad (1)$$

where d_i are the distances between the intersection points of the HOLZ lines in both the experimental (expt) and simulated (theor) patterns, σ_i is the experimental average HOLZ-line width, N is the number of intersection points considered, and m the number of parameters to be determined. Although it has been shown that the HOLZ-lines patterns are best modeled using fully dynamical calculations, or degenerate perturbation theory,[14] kinematical calculations are generally used[10,15] because of their simplicity and computational speed, which is mandatory for mismatch evaluations through a best-fit procedure. In a fully kinematical approach the fitting procedure starts matching the HOLZ-lines pattern taken in the substrate with the high voltage as the unique fitting parameter. Then assuming the transferability of the high voltage from the substrate to the strained layers, the unknown lattice parameters can be determined.

In the case of $Si_{1-x}Ge_x$ alloys with $x<0.2$, it has been recently shown[10] that strain can be determined with an accuracy of the order of 10^{-4} if the effects of the zero-order Laue zone (ZOLZ) dispersion surface are taken into account in the kinematical calculations of the positions of the HOLZ lines. In particular, for the ⟨130⟩ zone axis characterized by a ZOLZ dispersion surface with only one branch significantly excited, the HOLZ-line pattern can be correctly simulated by a kinematical approach if a correction factor ΔE is applied to the actual high voltage E_0. The correction factor, defined by the difference between the actual and the effective high voltage (i.e., the one used in the simulations), can be evaluated if the eigenvalue of the most excited branch of the ZOLZ dispersion surface is calculated by zero-layer dynamical simulations. In order to achieve a comparable accuracy for $x>0.2$ many-beams dynamical calculations are needed.

In the present paper the best matching between the experimental and calculated patterns based on the kinematical approximation have been refined using many-beams dynamical calculations. The calculations have been performed solving the time-independent Schrödinger equation in the Bloch-wave formalism[9] using the EMS software,[16] including 14 and 32 zero- and second-order Laue zone beams, respectively (the first-order Laue zone is forbidden in diamond structures for this zone axis). A beam with half-convergence of 2.5 nm^{-1} and a maximum deviation parameter from the Bragg position $s_g^{\max}=0.2\,nm^{-1}$ has been used. Absorption has been taken into account using the Weickenmeier-Kohl scattering factors.[17]

D. LACBED static disorder determination

1. Effect of static disorder on electron scattering factors in $Si_{1-x}Ge_x$ alloys

Generally, in the case of a perfectly substitutional disordered binary alloy A_xB_{1-x}, like SiGe alloys, small local distortions in the crystalline lattice must exist because of the fact that the atoms are of different sizes. For the same coordination shell, AA, AB, and BB pairs have different average interatomic distances producing the so-called static disorder.

In order to study the static disorder in crystalline, perfectly disordered, binary alloys with the measurements of diffracted intensities, it is necessary to adopt a model for the calculation of the structure factors, as the random distribution in the lattice of different atomic species A and B destroy the spatial periodicity of the crystal structure. However, in the case of a perfectly substitutional disordered A_xB_{1-x} alloy, an average lattice can be defined and the total scattered intensity distribution near the reciprocal-lattice point **g** can be written as[18]

$$J_{g,\mathrm{tot}}^{AB}(s)=(V_g^{AB})^2+[\Delta V^{AB}(s)]^2. \qquad (2)$$

TABLE I. Electron scattering factors V_{880}, for $\mathbf{g}=880$ ($g=20.8\,\mathrm{nm}^{-1}$ in Si), computed for silicon and germanium according to Wickenmayer and Kohl (Ref. 17) and for cubic $Si_{1-x}Ge_x^*$ according to Eq. (7) (see the text). The pure element thermal Debye-Waller factors, $B_T=2\pi^2\langle u_x^2\rangle_{\mathrm{th}}$, have been taken from the literature (Ref. 20). The Debye temperatures have been computed using Eqs. (8) and (9) (see the text). The values obtained for Si and Ge are in agreement with those used in x-ray diffraction experiments (Ref. 22). The last column reports the ratio between the scattering factors for the alloys without static disorder and the one for Si, which will be adopted as a normalization factor in static disorder measurements [see Eq. (11) of the text].

	Θ_D (K)	B_T (nm^2)	V_{880} (V)	$N(x)=(V_{880}^{Si_{1-x}Ge_x^*}/V_{880}^{Si})^2$
Silicon	538	0.001 15	0.4372	1
$Si_{0.9}Ge_{0.1}^*$	494	0.001 17	0.4826	1.219
$Si_{0.8}Ge_{0.2}^*$	457	0.001 18	0.5268	1.452
$Si_{0.7}Ge_{0.3}^*$	427	0.001 20	0.5697	1.698
Germanium	292	0.001 43	0.8207	3.524

Here **g** is the reciprocal lattice vector, s is the reciprocal-lattice scattering vector, and V_g^{AB} is the gth component of Fourier transform of the electrostatic potential $\langle V^{AB}(r)\rangle$ of the average lattice, which gives rise to the coherent intensity at the Bragg positions. The term $[\Delta V^{AB}(s)]^2$ represents the square of the Fourier transform of the deviation of the real structure from the average lattice, $\langle \Delta V^{AB}(r)\rangle$, which is in general a nonperiodic intensity (diffuse scattering).

In the case of an A_xB_{1-x} alloy, the average scattering factors is represented by[19]

$$V_g^{AB}=xV_g^A\exp[-M^Ag^2]+(1-x)V_g^B\exp[-M^Bg^2], \quad (3)$$

where V_g^i and $\exp[-M^i]$ are the atomic scattering factor and Debye-Waller factor of each constituent atom i (i stands for an A or B atom), respectively, and g is the modulus of the reciprocal-lattice vector of the diffracted beam. In an isotropic approximation M^i is given by[19]

$$M^i=\tfrac{2}{3}\pi^2\langle u^2\rangle^i=2\pi^2\langle u_x^2\rangle^i, \quad (4)$$

where $\langle u^2\rangle^i$ is the mean-square displacement of the atom i and $\langle u_x^2\rangle^i$ is its component along the direction parallel to **g**.

In a perfectly disordered alloy, like $Si_{1-x}Ge_x$ alloys, the following simplification holds:[19]

$$M^A=M^B=M(x), \quad (5)$$

and $M(x)$ consists of two terms:

$$M(x)=2\pi^2\langle u_x^2(x)\rangle_t+2\pi^2\langle u_x^2(x)\rangle_s=B_T(x)+L_H(x), \quad (6)$$

where $\langle u_x^2(x)\rangle_t$ is the *thermal* mean-square atomic displacement due to the lattice vibration, and $\langle u_x^2(x)\rangle_s$ is the *static* mean-square atomic displacement due to the size difference of constituent atoms as a function of Ge atomic fraction x. In this description the scattering factor for the $Si_{1-x}Ge_x$ alloys is given by

$$V_g^{Si_{1-x}Ge_x}=[(1-x)V_g^{Si}+xV_g^{Ge}]\exp[-L_H(x)g^2]$$
$$=V_g^{Si_{1-x}Ge_x^*}\exp[-L_H(x)g^2], \quad (7)$$

where x is the Ge atomic fraction, V_g^{Si}, V_g^{Ge}, $V_g^{Si_{1-x}Ge_x^*}$ are the electron scattering factors corrected for the appropriate thermal Debye-Waller factor $B_T(x)$ computed according to Weickenmayer and Kohl.[17] The apex* indicates the scattering factor for the SiGe alloy calculated neglecting the effect of static disorder. In this approximation we found that in real $Si_{1-x}Ge_x$ alloys the contribution of static disorder to the scattering factor is given by the factor $\exp[-L_H(x)g^2]$. Then the information on static disorder is mainly present in high-angle diffracted beams.

The thermal Debye-Waller factors B_T of the $Si_{1-x}Ge_x$ alloys can be determined from the thermal root-mean-square atomic displacement $\langle u_x^2(x)\rangle_{\mathrm{th}}$:

$$\langle u_x^2(x)\rangle_{\mathrm{th}}=\frac{3h^2}{4\pi^2k_BM\mu(x)\Theta_D(x)}\times\left\{\frac{1}{4}+\frac{T^2}{\Theta_D^2(x)}\int_0^{\Theta_D(x)/T}\frac{y\,dy}{e^y-1}\right\}, \quad (8)$$

where h and k_B are the Planck and Boltzmann constants, respectively, M is the atomic mass unit, T is the Kelvin temperature, and $\mu(x)$ and $\Theta_D(x)$ are the concentration-dependent atomic weight and Debye temperature of the alloy, respectively.[20] According to Shirley and Fisher,[19] the quantities $\mu(x)$ and $\Theta_D(x)$ for alloys without short-range order can be reasonably obtained from the following equations:

$$\mu(x)=(1-x)\mu^{Si}+x\mu^{Ge},$$
$$(\Theta_D(x))^2=[(1-x)\mu^{Si}(\Theta_D^{Si})^2+x\mu^{Ge}(\Theta_D^{Ge})^2]/\mu(x). \quad (9)$$

The choice of the appropriate Θ_D^{Si} and Θ_D^{Ge} values is not trivial because the numeric value of Θ_D depends on the probe used for its measurement. In fact the phonon spectrum is weighted differently in diffraction experiments and in specific-heat measurements.[21] The Θ_D values adopted here are deduced from the Debye-Waller factors of Si and Ge specific for electron diffraction reported in the literature.[20] The adopted Debye temperature, the Debye-Waller factors, and the electron scattering factors for Si, Ge, and $Si_{1-x}Ge_x^*$ alloys are reported in Table I.

2. Experimental method for static disorder determination

The analysis of static disorder can be performed with the large-angle convergent beam electron-diffraction (LACBED)

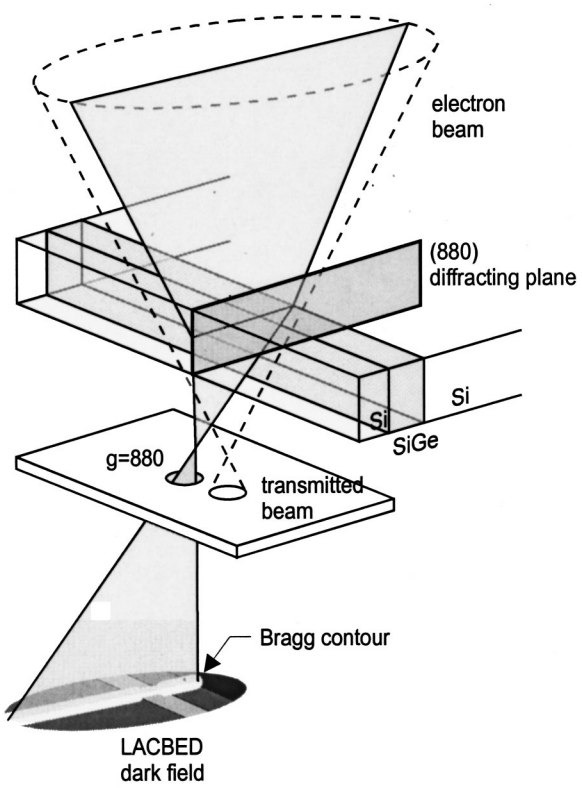

FIG. 3. Experimental LACBED geometry used in static disorder measurements. The sample is oriented along the [4-41] zone axis where the (880) planes are Bragg diffracted giving rise to the (880) diffracted beam selected by an aperture. The (880) dark field LACBED (DFLACBED) pattern and the corresponding Bragg contour are formed in the recording plane.

technique available in a transmission electron microscope (TEM). In this technique a probe with a large convergence angle is focused in a plane slightly below or above the sample, thus forming a diffraction pattern (instead of an intermediate image) in the plane of the selected area aperture. This aperture can then be used to isolate one reflection and thus prevent overlapping of the diffracted beams in the final detection plane.[23] In these patterns different regions of the sample, with lateral dimensions of the order of the probe diameter, contribute to different parts of the *same* diffraction pattern, thus allowing an accurate comparison between the diffracted intensity coming from different areas of the sample with a spatial resolution of the order of 10 nm. It will be shown that this peculiarity allows us to determine the static disorder in the SiGe layers from a TEM cross section of the heterostructure using a method similar to the one reported for the Si(H) system obtained by ion implantation.[11]

In Fig. 3 a sketch of the experimental geometry used for the measurement of L_H in a (1-10) TEM cross section is reported. The sample is tilted by about 10° toward the [4-41] zone axis where the high-angle reflection $\mathbf{g}=880$ ($g=20.8\,\mathrm{nm}^{-1}$ in Si) can be brought into the Bragg position. The corresponding Bragg contour (defined as the locus of the Bragg peak in the dark field LACBED (DFLACBED) pattern) is perpendicular to the Si/SiGe interfaces and can be quantitatively analyzed. This reflection is not sensitive to atomic displacements $\mathbf{r}$ along both the [001] and [1-10] directions normal to the free surfaces of the bulk sample and of the TEM cross section, respectively, because of the $\mathbf{g}\cdot\mathbf{r}=0$ rule. Unwanted effects on the diffracted intensity due to the stress relaxation and to the specimen preparation can then be reasonably minimized and the static disorder in planes parallel to the interface determined.

In detail the method is based on the quantitative analysis of the rocking curves of the (880) reflection obtained from intensity line scans across the Bragg contour. It will be shown that the ratio (R ratio) between the *integrated intensity* of the rocking curve in Si crystal, A_g^{Si}, and in the alloy, $A_g^{\mathrm{Si}_{1-x}\mathrm{Ge}_x}$, is sensitive to the static disorder parameter L_H. In fact, starting from a simple kinematical approximation, the following equation for the R ratio holds:

$$R(x)\equiv\frac{A_g^{\mathrm{Si}}}{A_g^{\mathrm{Si}_{1-x}\mathrm{Ge}_x}}=\left(\frac{V_g^{\mathrm{Si}}}{V_g^{\mathrm{Si}_{1-x}\mathrm{Ge}_x}}\right)^2\frac{t^{\mathrm{Si}}}{t^{\mathrm{Si}_{1-x}\mathrm{Ge}_x}},\qquad(10)$$

where $t^{\mathrm{Si}}/t^{\mathrm{Si}_{1-x}\mathrm{Ge}_x}$ is the ratio between the local thickness of the cross-section TEM sample in the silicon substrate and in the alloy that can be determined in an independent way.[24] From Eq. (10) the static disorder parameter L_H can be determined as a function of the Ge atomic fraction x, once the electron scattering factors are expressed as in Eq. (7):

$$\begin{aligned}L_H(x)&=\frac{1}{2g^2}\ln\left[\frac{A^{\mathrm{Si}}}{A^{\mathrm{Si}_{1-x}\mathrm{Ge}_x}}\frac{t^{\mathrm{Si}_{1-x}\mathrm{Ge}_x}}{t^{\mathrm{Si}}}\left(\frac{V_g^{\mathrm{Si}_{1-x}\mathrm{Ge}_x^*}}{V_g^{\mathrm{Si}}}\right)^2\right]\\&=\frac{1}{2g^2}\ln\left[R(x)\frac{t^{\mathrm{Si}_{1-x}\mathrm{Ge}_x}}{t^{\mathrm{Si}}}N(x)\right].\qquad(11)\end{aligned}$$

In Eq. (11) the ratio $N(x)=(V_g^{\mathrm{Si}_{1-x}\mathrm{Ge}_x^*}/V_g^{\mathrm{Si}})^2$ is a normalization factor which allows us to obtain the static disorder parameter by direct comparison between the integrated intensities measured in Si and in the SiGe layers available in a DFLACBED pattern taken on the TEM cross section. The normalization factor $N(x)$ is determined from the ($\mathbf{g}=880$), Si and $\mathrm{Si}_{1-x}\mathrm{Ge}_x^*$ electron scattering factors and is reported in Table I.

Unfortunately the relationship between the reduction of the diffracted intensity and L_H is only at a first-order approximation predictable from Eq. (11) on the basis of the simple kinematical theory. In fact many-beams effects, typical of the electron-diffraction process, occur even when the samples are oriented along a quite ''sparse'' zone axis like [4-41].[11] A more accurate determination of the L_H parameter needs a treatment of the integrated intensities based on the many-beam dynamical diffraction process.

This task has been tackled solving the time-independent Schrödinger equation in the Bloch-wave formalism[9] in the geometry shown in Fig. 3 for different SiGe structures. A half-convergence angle of 10 nm^{-1} and a Laue circle centered at the $\mathbf{g}=440$ position ($\mathbf{g}=880$ in the Bragg position) has been assumed to simulate the DFLACBED pattern. In addition to the silicon structure, and to the three $\mathrm{Si}_{1-x}\mathrm{Ge}_x^*$ ($x=0.1$, $x=0.2$, $x=0.3$) structures without static disorder, two alloy crystal structures for each atomic Ge fraction x, with two plausible different levels of static disorder $L_H^{(1)}(x)$, $L_H^{(2)}(x)$, have been considered (see Table II).

TABLE II. Static disorder parameters adopted in the many-beam dynamical simulations of DFLACBED patterns of $Si_{1-x}Ge_x$ alloys. The last row reports the resulting quasikinematical correction factors $b(x)$ for the thickness of the cross-section sample ranging from 150 to 250 nm.

	$x=0.1$	$x=0.2$	$x=0.3$
$L_H^{(1)}$ (nm^2)	2×10^{-4}	3×10^{-4}	4×10^{-4}
$L_H^{(2)}$ (nm^2)	4.5×10^{-4}	7×10^{-4}	1×10^{-3}
$b(150<t<250\,\text{nm})$	1.36	1.34	1.41

The simulations have been performed using the EMS software,[16] including 15 zero-order Laue zone beams and 20 first-order Laue zone beams with a maximum deviation parameter from the Bragg position $s_g^{\max}=0.4\,\text{nm}^{-1}$. Absorption has been taken into account using the Weickenmeier-Kohl scattering factors.[17] The integrated intensities have been calculated from line scans across the simulated Bragg contour. Convergence in the Bloch-wave calculations has been determined checking the invariance of the integrated intensities with respect to the increase of the number of the diffracted beams.

Figures 4 and 5 summarize the results of these calculations. In Fig. 4 it is shown that the integrated intensity increases almost linearly with the thickness t of the sample for

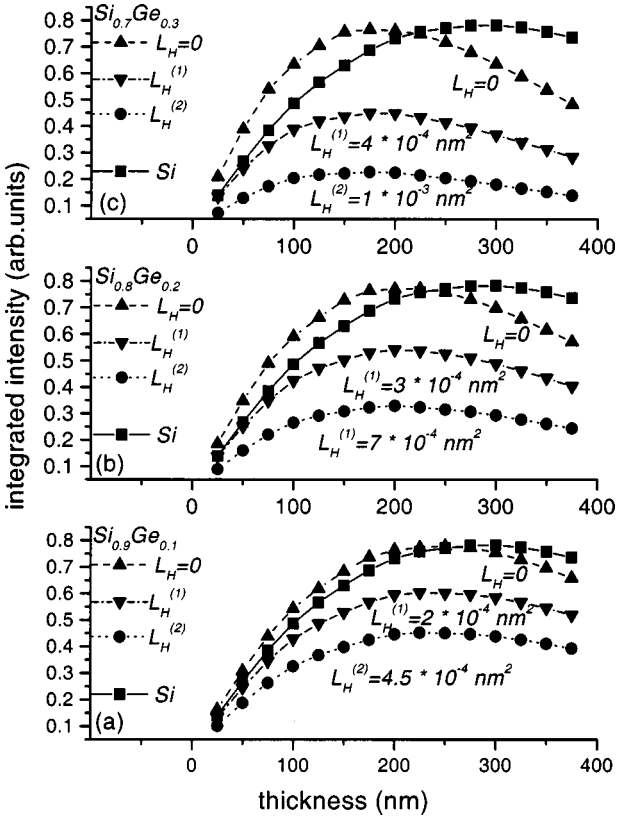

FIG. 4. Results of the many-beams simulation of the integrated intensity in a (880) Bragg contour in silicon and in $Si_{1-x}Ge_x$ alloys without static disorder and with a different level of static disorder: (a) $Si_{0.9}Ge_{0.1}$, (b) $Si_{0.8}Ge_{0.2}$, and (c) $Si_{0.7}Ge_{0.3}$. Each point represents the integrated intensity of the (880) reflection for the correspondent thickness of the sample resulting from the many-beam simulation of the diffraction pattern.

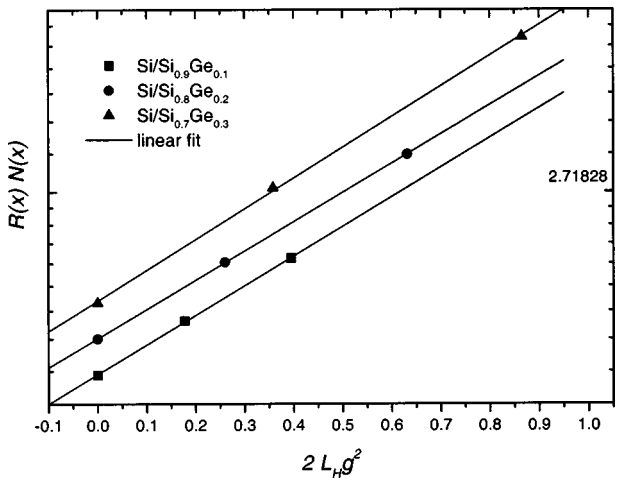

FIG. 5. Logarithmic plot of the calculated normalized ratio $R(x)N(x)$ between integrated intensity in Si and in $Si_{1-x}Ge_x$ alloys vs the static disorder parameter for a 200-nm-thick sample.

$t<100\,\text{nm}$ as expected from the kinematical theory. For $t>100\,\text{nm}$ the intensity deviates from the kinematical predicted behavior. However, for t ranging from 150 to 250 nm, suitable for DFLACBED experiments at 100 keV, the integrated intensities and then the corresponding R ratio are weakly dependent from t. In Fig. 5 is reported the logarithm of integrated intensity versus the static disorder parameter L_H for each Ge concentration (for $t=200\,\text{nm}$). It is shown that the normalized integrated intensity ratio between the Si and SiGe alloys depends exponentially from L_H, in the following way:

$$R(x)N(x)\equiv\frac{A_g^{\text{Si}}}{A_g^{\text{Si}_{1-x}\text{Ge}_x}}N(x)=\exp[2b(x)g^2L_H(x)]. \tag{12}$$

For thickness in the range 150–250 nm $b(x)$ values are *nearly constant* for each Ge concentration (see Table II). The values of $b(x)$ define the correction factors that must be applied to the logarithm of the intensity ratio reported in Eq. (11) in order to determine L_H in a ''quasikinematical'' approximation. Due to the very small lateral dimensions of the SiGe layers (20 nm) and to the weak dependence of the integrated intensity from the thickness of the sample, the R ratio can be considered, in a good approximation, as independent from t. Then for thickness of the TEM sample ranging from 150 to 250 nm it is possible to deduce L_H from the following formula:

$$L_H(x)=\frac{1}{2g^2b(x)}\ln\left[\frac{A_g^{\text{Si}}}{A_g^{\text{Si}_{1-x}\text{Ge}_x}}\left(\frac{V_g^{\text{Si}_{1-x}\text{Ge}_x^*}}{V_g^{\text{Si}}}\right)^2\right]$$

$$=\frac{1}{2g^2b(x)}\ln[R(x)N(x)]. \tag{13}$$

It must be stressed here that the diffuse scattering intensity is not taken into account in the calculations. Nevertheless, according to Tsuda and Tanaka[25] we can suppose that for high-angle reflections the contribution to the intensity of

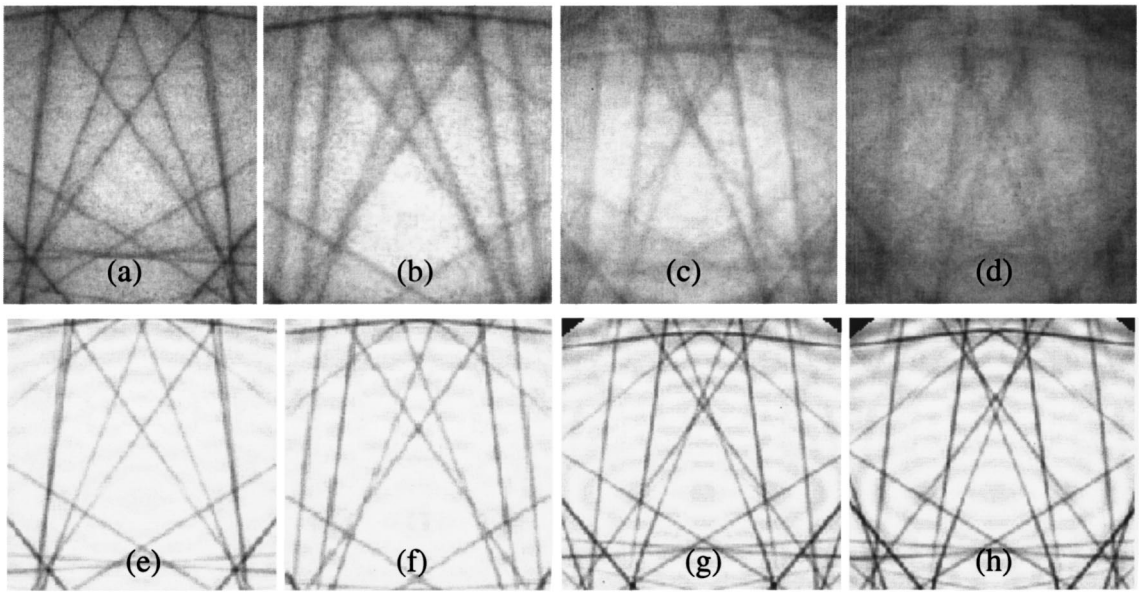

FIG. 6. Experimental and simulated ⟨130⟩ CBED-HOLZ line patterns, (a)–(e) silicon, (b)–(f) $Si_{0.9}Ge_{0.1}$, (c)–(g) $Si_{0.8}Ge_{0.2}$, (d)–(h) $Si_{0.9}Ge_{0.3}$.

both the diffuse scattering and the inelastic scattering can be reasonably removed from the experimental patterns by linear background subtraction.

III. RESULTS

The ⟨130⟩ HOLZ-lines patterns recorded in the silicon substrate and in the SiGe layers are reported in Figs. 6(a)–6(d). These patterns have been analyzed with the procedure reported in Sec. II C. The actual high voltage (ht $=99.75$ keV) has been determined from best-fit matching of the silicon HOLZ-lines patterns [Fig. 6(a)] with dynamical simulations [Fig. 6(e)]. Then the alloy lattice parameters have been determined by the best fit of experimental patterns with kinematical simulations of the patterns through the minimization of χ^2 [see Eq. (1)]. A refinement of the lattice parameters has been performed using the same minimization criteria applied to the comparison between dynamical simulation and experimental patterns. The final simulations are reported in Figs. 6(f)–6(h). The resulting lattice parameters are reported in Table III (in the second to fourth columns). The large experimental errors are due to the broadening of the HOLZ lines produced both by static disorder and stress relaxation. The angle γ (fourth column) allows us to confirm the coherence between the SiGe layer and the Si substrate. In fact it can be shown from simple geometry that the shear strain deduced from the departure of γ from 90° depends on the relaxation of the stress field along the normal to the cross-section plane and is related to the length of the a and b edges of the unit cell. In particular, if the lattice parameter in the plane of the interface is equal to the silicon lattice parameter, the following simple relationship holds: $\Delta a/a = \Delta b/b = -\Delta\gamma/2$. All the HOLZ-line patterns of our experiment have been fit with this constraint or with a very small deviation from it. The data of Table III are then compatible with an in-plane lattice parameter $a_{\parallel}$ equal to $a_{Si} = 0.5429$ nm, which is the silicon lattice constant at a temperature of -170 °C. The lattice parameters of the alloy, measured along different crystallographic directions from a single HOLZ-line pattern, can then be properly combined in order to compensate for the systematic error caused by the extra-relaxation induced by the thinning process. In fact, according to the method proposed by Balboni *et al.*,[10] it is possible to deduce the perpendicular mismatch $m_{\perp} = (a_{\perp} - a_{Si})/a_{Si}$ and the misfit parameter $f = (a_R - a_{Si})/a_{Si}$ from the following relationship:

$$m_{\perp} = m_{001}^{\mathrm{CBED}} + \frac{\nu_2}{1-\nu_1} m_{110}^{\mathrm{CBED}} = \frac{1+\nu}{1-\nu} f. \tag{14}$$

Here $m_{001}^{\mathrm{CBED}} = (c - a_{Si})/a_{Si}$ is the mismatch along the [001] growth direction and

TABLE III. Results of strain measurements in $Si_{1-x}Ge_x$ heterostructures. The lattice constants a, b, c, and γ are determined from the best fit of ⟨130⟩ CBED patterns. The perpendicular mismatch $m_{\perp}$ is determined according to Eq. (14) (see the text). f is the misfit parameters and a_R is the (equilibrium) lattice parameter of the cubic relaxed alloy for each concentration.

	$a=b$ (10^{-4} nm)	c (10^{-4} nm)	γ (deg)	$m_{\perp}$ (10^{-3})	f (10^{-3})	a_R (10^{-4} nm)
$x=0.1$	5432 ± 4	5460 ± 3	89.96 ± 0.05	6.2 ± 1.1	3.45 ± 0.8	5448 ± 3
$x=0.2$	5435 ± 5	5490 ± 3	89.90 ± 0.05	12.6 ± 1.5	7.1 ± 0.8	5467 ± 4
$x=0.3$	5435 ± 6	5520 ± 5	89.90 ± 0.05	17.2 ± 1.8	9.7 ± 1.0	5482 ± 6

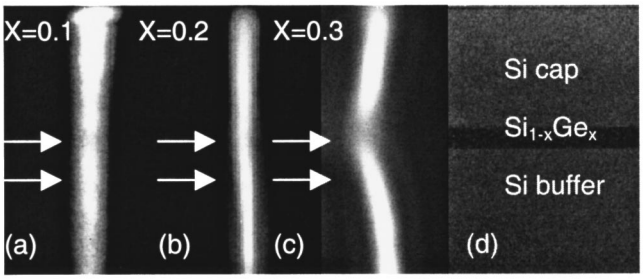

FIG. 7. DFLACBED patterns of heterostructures showing the (880) Bragg contour which crosses the Si/SiGe interfaces: (a) $Si_{0.9}Ge_{0.1}$, (b) $Si_{0.8}Ge_{0.2}$, and (c) $Si_{0.7}Ge_{0.3}$. (d) is a bright field image reported for depth scale calibration. The arrows mark the depth where line scans across the Bragg contour have been taken for integrated intensity analysis.

$$m_{110}^{\mathrm{CBED}}=\frac{\sqrt{b^2-(a_{\mathrm{Si}}/\sqrt{2})^2}-a_{\mathrm{Si}}/\sqrt{2}}{(a_{\mathrm{Si}}/\sqrt{2})}$$

is the mismatch along the direction normal to the TEM cross-section plane, caused by the extra-relaxation induced by the thinning process, both determined from the same CBED pattern. The elastic constants $\nu_2=0.36$ and $\nu_1=0.064$ are the Poisson coefficient for stress applied along a [110] direction relaxed along the [001] and [1-10] directions, respectively.[26] The elastic constant $\nu=0.28$ is the Poisson coefficient for stress applied along the [100] direction and relaxed along a perpendicular [001] direction which is equal to the isotropic value ν.[26] It is worth noting here that for the sample thickness used in these experiments (about 200 nm), the relaxed fraction is very small. From the measurements of both $m_\perp$ and $a_\parallel$, the perpendicular lattice parameter $a_\perp$, and the misfit f between the relaxed SiGe alloy and the Si substrate can be determined. From f the relaxed alloy lattice parameters $a_R(x)$ can be obtained (see Table III) thus allowing the determination of the in-plane $\varepsilon_\parallel=(a_\parallel-a_R)/a_R$ and perpendicular $\varepsilon_\perp=(a_\perp-a_R)/a_R$ strain, respectively.

In Fig. 7(a)–7(c) the Bragg contours of the (880) reflection taken from the DFLACBED patterns are reported relative to the three investigated samples. The position of the SiGe layer can be determined by comparison with the bright field image reported in Fig. 7(d). Arrows indicate the depths where intensity line scans have been recorded in order to obtain the rocking curves used in the static disorder determination. In the $Si_{0.7}Ge_{0.3}$ DFLACBED of Fig. 7(c) a bending of the Bragg contour is evident at the $Si/Si_{0.7}Ge_{0.3}$ interface that could reasonably be ascribed to the presence of shear strains induced by the thinning of the cross-section TEM sample,[12] or to small strain relaxation in the plane of the Si/SiGe interface. We ascribe the bending of the Bragg contour to the shear strain induced in the thinning step of the TEM cross section because we do not observe misfit dislocations in (diffraction contrast) plan-view images and because the CBED strain measurements reasonably fit with an in-plane lattice parameter equal to the one of the silicon substrate. The effect of this bending is then neglected in the evaluation of intensity ratio as shear strains are expected do not to affect the volume of the unit cell.

In Fig. 8 the rocking curves obtained by plotting the result of the line scans across the Bragg contour after a linear background subtraction are reported. From these rocking curves, following the procedure reported in Sect. III D, we have determined the ratio $R(x)$ between the integrated intensities in the substrate and in the SiGe layers for each Ge atomic fraction. These ratios inserted in Eq. (13), together with the normalization factor $N(x)$ and the correction factors $b(x)$, allow us to determine $L_H(x)$ and $\langle u_x^2(x)\rangle_s^{\mathrm{exp}}$. The results are summarized in Table IV.

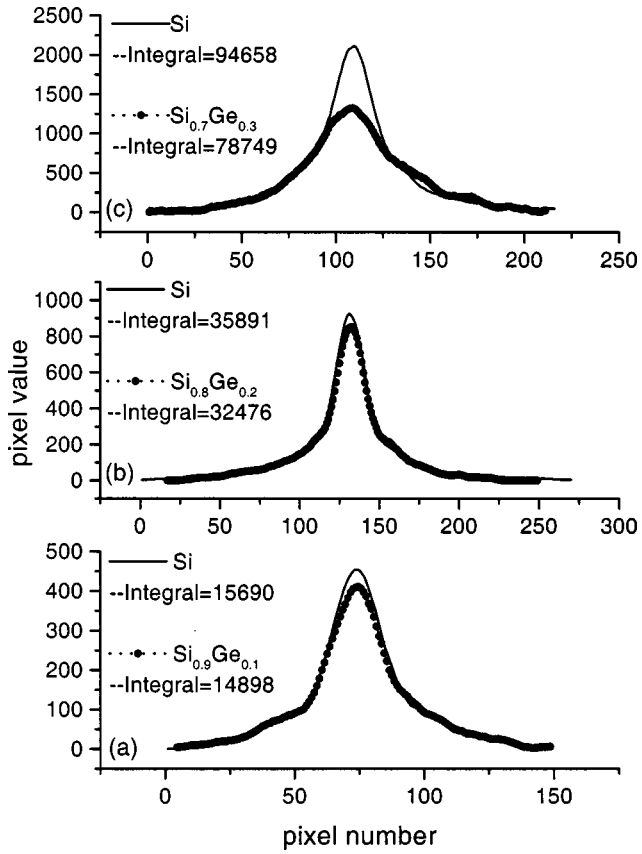

FIG. 8. Experimental rocking curves obtained from line scans across the (880) Bragg contour after a linear background subtraction; (a) $Si_{0.9}Ge_{0.1}$, (b) $Si_{0.8}Ge_{0.2}$, and (c) $Si_{0.7}Ge_{0.3}$.

IV. DISCUSSION

It is known from the literature that the behavior of the relaxed lattice constant $a_R(x)$ as a function of the Ge concentration slightly deviates (in the negative sense) from Vegard's law.[1,3,4] This approximation, when it is written for atoms described as hard (incompressible) spheres with a ra-

TABLE IV. Static disorder measurements: $R(x)$ is the experimental ratio between integrated intensity in Si and $Si_{1-x}Ge_x$ layers; $N(x)=(V_{880}^{Si_{1-x}Ge_x^*}/V_{880}^{Si})^2$ is the normalization factor, $b(x)$ represents the quasikinematical correction factor.

	$R(x)$	$N(x)$	$b(x)$	L_H (10^{-4}) nm^2	$\langle u_x^2\rangle_{\mathrm{static}}^{\mathrm{expt}}$ (10^{-5}) nm^2
x=0.1	1.053	1.219	1.36	2.12	1.1±0.5
$x=0.2$	1.105	1.452	1.34	4.07	2.1±0.5
$x=0.3$	1.202	1.698	1.41	5.83	2.95±0.5

IV. DISCUSSION

It is known from the literature that the behavior of the relaxed lattice constant $a_R(x)$ as a function of the Ge concentration slightly deviates (in the negative sense) from Vegard's law.[1,3,4] This approximation, when it is written for atoms described as hard (incompressible) spheres with a ra-

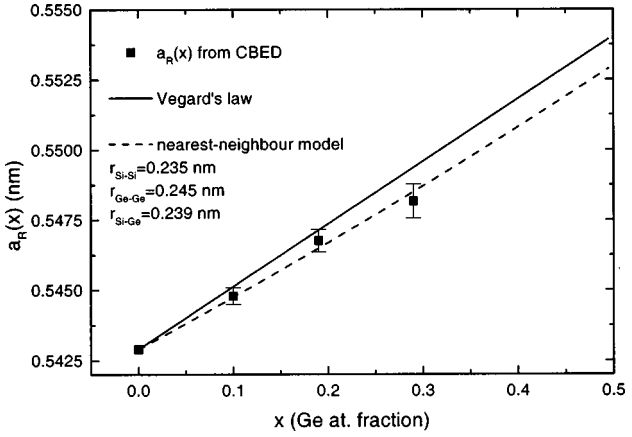

FIG. 9. Plot of the relaxed lattice parameter for $Si_{0.9}Ge_{0.1}$, $Si_{0.8}Ge_{0.2}$, and $Si_{0.7}Ge_{0.3}$ alloys, determined from CBED-HOLZ lines measurements as a function of the Ge atomic fraction. The nearest-neighbor model and Vegard's law are reported for comparison. The bond lengths used in the nearest-neighbor model are reported in the inset.

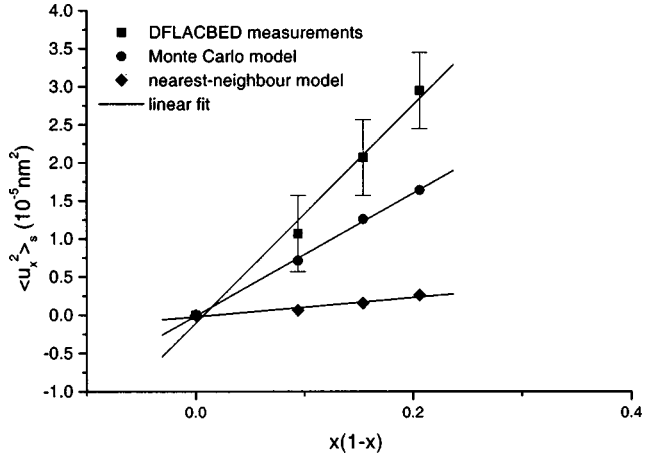

FIG. 10. Plot of the atomic mean-square static displacement determined from DFLACBED, from Monte Carlo simulations of the relaxed alloy, and from the nearest-neighbor model, as a function of the product of Si and Ge atomic content.

dius equal to the natural bond length of the Si and Ge, allows us to deduce the relaxed lattice constant by linear interpolation between the two end-point structures of Si and Ge, $a_R(x)_{\text{Vegard}} = x a_{\text{Ge}} + (1-x) a_{\text{Si}}$.

In Fig. 9 are reported the lattice constants of the relaxed alloys as deduced from strain measurements together with Vegard's law data (continuous line) obtained using the values of the lattice constants of Si, $a_{\text{Si}} = 0.5429\,\text{nm}$, and Ge, $a_{\text{Ge}} = 0.5652\,\text{nm}$, at $-170\,^{\circ}\text{C}$ (Ref. 1) (which is the temperature of the sample during the CBED analysis) as an end-point structure. According to literature, our data slightly deviate from Vegard's law, in particular for the $Si_{0.7}Ge_{0.3}$ sample.

A better description of our experimental data can be obtained using the nearest-neighbor model.[6,27] Indeed, following this approximation, it is possible to deduce the mean bond length $\langle r(x)\rangle^{\text{NN}}$ of the relaxed alloy by weighting the Si-Si (r_{Si}), Si-Ge (r_{SiGe}), Ge-Ge (r_{Ge}) bond lengths with the distribution function of the occurrence of each bond length. This function is equal to the product between the atomic fractions of the bonded species times the number of bonded species:

$$\langle r(x)\rangle^{\text{NN}} = x^2 r_{\text{Ge}} + (1-x)^2 r_{\text{Si}} + 2x(1-x) r_{\text{SiGe}}. \quad (15)$$

From Eq. (15) the mean relaxed lattice constant is determined as $a(x)_R^{\text{NN}} = (4/\sqrt{3})\langle r(x)\rangle^{\text{NN}}$. In Fig. 9 this quantity (dashed line) is reported assuming, in agreement with EXAFS measurements,[5–8] the following Si-Si, Ge-Ge, and the Si-Ge bond lengths: $r_{\text{Si}} = 0.235\,\text{nm}$, $r_{\text{Ge}} = 0.245\,\text{nm}$, and $r_{\text{SiGe}} = 0.239\,\text{nm}$. It is worth noting that the deviation from Vegard's law depends on the deviation of the r_{SiGe} value from the mean value obtained from the pure elements bond lengths.

The previous measurements indicates that the measured lattice parameters of the 20 nm $Si_{1-x}Ge_x$ alloys, for the atomic concentrations studied in the present paper, are consistent with an assumption of a negligible variation of Si-Si, SiGe, and Ge-Ge bond length with Ge atomic fraction in agreement with some EXAFS measurements.[5–8] Of course we cannot exclude the existence of a bond-length variation with the Ge concentration on the scale of $10^{-4}\,\text{nm}$ as expected from theoretical calculations[28] and observed in a EXAFS experiment on a 200-nm Ge-rich alloy, hydrogen contamination free, grown by molecular beam epitaxy.[7] Then, from the macroscopic elasticity-theory point of view our films are, within the experimental errors, similar to thicker films.

The presence in the alloys of bonds with different lengths is confirmed from the second set of experimental data given by LACBED experiments on the mean-square atomic displacements reported in Fig. 10. These data, like the mean bond lengths of Eq. (15), depend on the Ge content following a regular solution model ($\langle u_x^2(x)\rangle_s^{\text{expt}} = Cx(1-x)$ with $C = 1.4\times10^{-4} \pm 0.1\,\text{nm}^2$). We attempt to apply the nearest-neighbor model that reasonably fits the lattice parameters measurements to describe the behavior of this parameter with the Ge content x. The diamonds of Fig. 10 represent the $\langle u_x^2\rangle_s^{\text{NN}}$ values calculated according to the following relationship:

$$\begin{aligned}\langle u_x^2(x)\rangle_s^{\text{NN}} = 1/3\langle u^2(x)\rangle_s^{\text{NN}} = 1/3[&(r_{\text{Si}} - \langle r(x)\rangle^{\text{NN}})^2(1-x)^2 \\ &+ (r_{\text{Ge}} - \langle r(x)\rangle^{\text{NN}})^2 x^2 \\ &+ 2(r_{\text{SiGe}} - \langle r(x)\rangle^{\text{NN}})^2 x(1-x)]. \quad (16)\end{aligned}$$

It is quite evident that the model does not fit the experimental observation of the static disorder. This suggests that the microscopic interpretation of the macroscopic elasticity theory in terms of bond stretch only, cannot describe the microscopic state of disorder caused by the presence of different bond lengths in the mean strained unit cell and observed in LACBED experiment.

Different and slightly better results are obtained by generating the relaxed SiGe alloy structure by Monte Carlo calculations in a way similar to the one reported by Fabbri *et al.*[3] that correctly describes the deviation from Vegard's law experimentally observed in the relaxed lattice parameter measurements. Here the only difference with respect to that case is in the definition of the starting silicon lattice as a parallelepiped limited by {110} (and not {100}) planes and

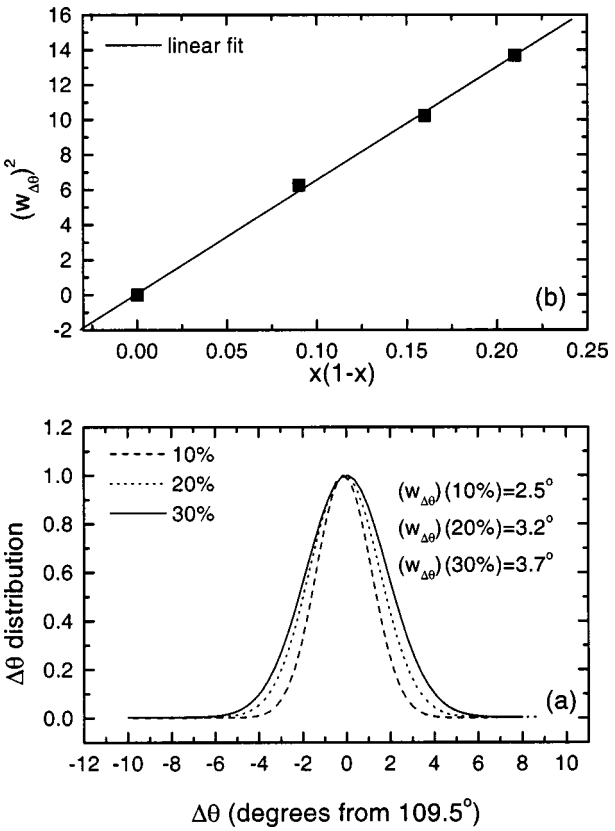

FIG. 11. (a) Monte Carlo results on the bond angle distribution for relaxed $Si_{0.9}Ge_{0.1}$, $Si_{0.8}Ge_{0.2}$, and $Si_{0.7}Ge_{0.3}$ alloys. (b) Correlation between the square of the distribution width and the product of Si and Ge atomic content.

composed of 44 539 atoms considered as rigid spheres. This modification is, in principle, needed because we measure the static disorder along a ⟨110⟩ direction. The procedure for the generation of the alloys are then summarized in the following points.

(i) A given fraction of Si atoms is replaced by Ge atoms in a completely random way.

(ii) The solid is expanded isotropically by the minimum amount required to host the Ge atoms at sites of a perfect diamond cubic lattice. This expansion, obtained minimizing the difference between the natural and the actual bond length by the last square method, is exactly that foreseen by Vegard's law.

(iii) Each atom is randomly chosen and its four nearest neighbors are radially displaced at the Si-Si, Si-Ge Ge-Ge natural bond lengths of pure materials.

(iv) Step (iii) is repeated until stability is reached for the sum of the squares of the differences between nominal and actual bond length. By tending this sum to zero, the values of the tetrahedral angles also tend to a stable configuration centered around the 109.5° [see Fig. 11(a)] with a root mean square w_θ^2, which scales regularly with the concentration as reported in and Fig. 11(b).

(v) Average (110) lattice planes are then traced through the new coordinates to the atoms and their mean distances are then evaluated as $\langle u_x^2(x)\rangle_s^{\mathrm{MC}}$ and reported as dots in the plot of Fig. 10.

TABLE V. Strain measured in the plane of the interface $[\varepsilon_\parallel=(a_\parallel-a_R)/a_R=(a_{\mathrm{Si}}-a_R)/a_R]$ and along the direction normal to the surface $[\varepsilon_\perp=(a_\perp-a_R)/a_R]$ of the $Si_{1-x}Ge_x$ films. Δr is the bond stretch, $\Delta\theta$ is the bond bend, and $\langle r\rangle$ is the mean bond length deduced from the relaxed lattice parameter determined in the CBED experiment, a_R.

	$\varepsilon_\parallel\,(10^{-4})$	$\varepsilon_\perp\,(10^{-4})$	$\Delta r/\langle r\rangle\,(10^{-3})$	$\Delta\theta$ (deg)
$x=0.1$	-35 ± 5	27 ± 5	-1.4 ± 1.2	-0.35 ± 0.1
$x=0.2$	-70 ± 5	56 ± 5	-2.6 ± 1.2	-0.7 ± 0.1
$x=0.3$	-97 ± 5	74 ± 5	-4.2 ± 1.2	-0.9 ± 0.1

The calculated $\langle u_x^2(x)\rangle_s^{\mathrm{MC}}$ values show a regular behavior with respect to the Ge content $[\langle u_x^2(x)\rangle_s^{\mathrm{MC}}=Dx(1-x)$ with $D=(8.1\times10^{-4})\pm0.2\,\mathrm{nm}^2]$ and, due to steps (iii) and (iv) in the generation of the alloy, are closer than the nearest-neighbor values to the experimental values. The remaining gap can then be reasonably ascribed to the strain present in the sample because, in the Monte Carlo construction of the relaxed alloy, the effect of the macroscopic strain on the microscopic rearrangement of atoms has been neglected.

This effect can be evaluated if the macroscopic strain data are connected to the microscopic structure considering, according to Woicik *et al.*,[8] the alloy as an ensemble of atoms bonded in virtual tetrahedrons. Due to strain both the length of the edges and internal angles of the tetrahedrons deviate from the relaxed value defining a bond bend $\Delta\theta$ in the plane of the interface (the same quantity in the planes perpendicular to the interface is found to be roughly equal to $\Delta\theta/2$ from simple geometry) and a bond stretch Δr. These microscopic parameters can be related to the measured perpendicular and parallel strain in the following way:

$$\varepsilon_\perp=(a_\perp-a_R)/a_R=(\Delta r/\langle r\rangle)-(\sqrt{2}/2)\Delta\theta,$$
$$\varepsilon_\parallel=(a_\parallel-a_R)/a_R=(\Delta r/\langle r\rangle)+(\sqrt{2}/4)\Delta\theta. \tag{17}$$

The measured strain values, the bond stretch, and the bond bend values deduced from Eq. (17) are reported in Table V. These results are in agreement with the literature data[8] relative to $x=0.21$ which gives a bond stretch of -8×10^{-4} nm and a bond bending $\Delta\theta=-0.8°$. This indicates that the macroscopic strain induces not only a small variation in the mean bond length $\langle r\rangle$ but also a (more important) change in the tetrahedral angle that seems to play a role on the $\langle u_x^2(x)\rangle_s^{\mathrm{expt}}$ of the strained alloy. Indeed, if we assume that the Monte Carlo calculations describe in a correct way the state of static disorder in the relaxed alloys, we can find the contribution to $\langle u_x^2(x)\rangle_s^{\mathrm{expt}}$ of the strain $\langle u_x^2(x)\rangle_s^{\mathrm{strain}}$ from the simple equation

$$\langle u_x^2(x)\rangle_s^{\mathrm{strain}}=\langle u_x^2(x)\rangle_s^{\mathrm{expt}}-\langle u_x^2(x)\rangle_s^{\mathrm{MC}}=Fx(1-x)=G|\Delta\theta|. \tag{18}$$

In Fig. 12(a) it is shown the regular behavior of $\langle u_x^2(x)\rangle_s^{\mathrm{strain}}$ with a slope $F=(6\pm1)\times10^{-4}\,\mathrm{nm}^2$ and in Fig. 12(b) the linear dependence of $\langle u_x^2(x)\rangle_s^{\mathrm{strain}}$ from $\Delta\theta$ with a slope $G=(-1.4\pm0.2)\times10^{-5}\,\mathrm{nm}^2/\mathrm{deg}$ is shown.

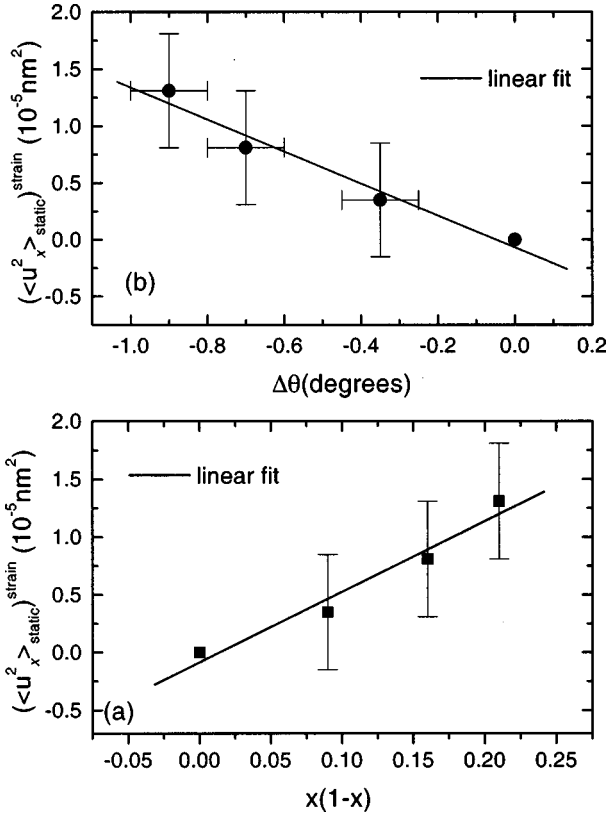

FIG. 12. Correlation between the component of the atomic displacements due to strain in a plane parallel to the interface and (a) the product of Si and Ge atomic content; (b) bond bend in a plane parallel to the interface determined from strain measurements.

V. CONCLUSIONS

In this paper we have studied the lattice strain and static disorder present in a $Si_{1-x}Ge_x$ alloy, forming $Si/(20\,nm)Si_{1-x}Ge_x/Si$ heterostructures and having a Ge atomic fraction x equal to 0.1, 0.2, and 0.3. The CBED and LACBED techniques have been used in order to perform structural analyses with a spatial resolution of about 10 nm comparable with the spatial scale involved in pseudomorphic heterostructures used in Si/SiGe applications. The measurements show the following.

(i) The strain in the films follows the macroscopic-elasticity theory; the relaxed lattice constants can be described in a frame of the nearest-neighbor solution model, thus having a regular dependence of the mean bond length from the Ge atomic fraction. This model describes the alloys combining the Si-Si, Ge-Ge, Si-Ge bond lengths with a negligible dependence on the Ge atomic fraction.

(ii) The determination of the lattice parameters of the strained heterostructures in the plane of the interface and along the direction normal to the surface allows the evaluation of the strain-induced bond bend $\Delta\theta$ and bond stretch Δr. The bond stretch is, in a first approximation, negligible with respect to the bond bend.

(iii) The atomic displacement determined from LACBED measurements are greater than the ones predicted by both the nearest-neighbor model (which only takes into account the differences in bond lengths, neglecting the effects of both bond bend and strain) and the Monte Carlo simulation of the structure of the relaxed alloys (which takes into account the differences in bond lengths and bond bend, but neglects the effect of strain).

(iv) The component of the atomic displacement related to the macroscopic strain has been determined, for each Ge concentration, as the difference between the experimental values and the ones computed by the Monte Carlo code. A linear correlation between the strain-induced atomic displacement and the strain-induced bond bend in the plane of the interface $\Delta\theta$ is found.

ACKNOWLEDGMENTS

The authors wish to thank Dr. M. R. Caymax (IMEC Leuven, Belgium) for the growth of the heterostructures. We also acknowledge A. Garulli (LAMEL Institute) for TEM specimen preparation and the staff of the Centro Interdipartimentale Grandi Strumenti (CIGS) of Modena University for skillful TEM technical assistance.

*Author to whom correspondence should be addressed FAX: ++39059367488. Electronic address. frabboni@unimo.it

[1] E. Kasper, *Properties of Strained and Relaxed Silicon Germanium* (INSPEC, London, 1995).
[2] P. M. Mooney, Mater. Sci. Eng., R. **17**, 105 (1996).
[3] R. Fabbri, F. Cembali, M. Servidori, and A. Zani, J. Appl. Phys. **74**, 2359 (1993).
[4] J. P. Dismukes, L. Ekstrom, and R. J. Pfaff, J. Phys. Chem. **68**, 3021 (1964).
[5] H. Kajiyama, S. Muramatsu, T. Shimada, and Y. Nishino, Phys. Rev. B **45**, 14 005 (1992).
[6] M. Matsuura, J. M. Tonnerre, and G. S. Cargill III, Phys. Rev. B **44**, 3842 (1991).
[7] D. B. Aldrich, R. J. Nemanich, and D. E. Sayers, Phys. Rev. B **50**, 15 026 (1994).
[8] J. C. Woicik, C. E. Bouldin, K. E. Miyano, and C. A. King, Phys. Rev. B **55**, 15 386 (1997).
[9] J. C. H. Spence and J. M. Zuo, *Electron Microdiffraction* (Plenum, New York, 1992).
[10] R. Balboni, S. Frabboni, and A. Armigliato, Philos. Mag. A **77**, 67 (1998).
[11] S. Frabboni and F. Gambetta, Phys. Rev. Lett. **81**, 3155 (1998).
[12] M. M. J. Treacy and J. M. Gibson, J. Vac. Sci. Technol. B **4**, 1458 (1986).
[13] J. M. Zuo, Ultramicroscopy **41**, 211 (1992).
[14] B. F. Buxton, Proc. R. Soc. London, Ser. A **350**, 335 (1976); P. M. Jones, G. M. Rackham, and J. W. Steeds, *ibid.* **354**, 197 (1977).
[15] D. M. Maher, H. L. Fraser, C. J. Humphreys, R. V. Knoell, and J. C. Bean, Appl. Phys. Lett. **50**, 574 (1987).
[16] P. A. Stadelmann, Ultramicroscopy **21**, 131 (1987).
[17] A. Weickenmeyer and H. Kohl, Acta Crystallogr., Sect. A: Found. Crystallogr. **47**, 590 (1991).
[18] J. M. Cowley, *Diffraction Physics* (North-Holland, Amsterdam, 1990), Chap. 12, p. 249.
[19] C. G. Shirley and R. M. Fisher, Philos. Mag. A **39**, 91 (1979).
[20] L. M. Peng, G. Ren, L. Dudarev, and M. J. Whelan, Acta Crystallogr., Sect. A: Found. Crystallogr. **52**, 456 (1996).

[21] B. W. Batterman and D. R. Chipman, Phys. Rev. **127**, 690 (1962).
[22] M. Deutsch and M. Hart, Phys. Rev. B **31**, 3846 (1985).
[23] M. Tanaka, J. Electron Microsc. **35**, 314 (1986).
[24] See, e.g., D. B. Williams and C. B. Carter, *Transmission Electron Microscopy* (Plenum, New York, 1996), Chap. 36, pp. 628–631.
[25] K. Tsuda and M. Tanaka, Acta Crystallogr., Sect. A: Found. Crystallogr. **51**, 7 (1995).
[26] W. A. Brantley, J. Appl. Phys. **44**, 534 (1973).
[27] J. W. Christian, *The Theory of Transformation in Metals and Alloys—Part I: Equilibrium and General Kinetic Theory*, 2nd ed. (Pergamon, Oxford, 1981), Chap. 6, p. 186.
[28] N. Mousseau and M. F. Thorpe, Phys. Rev. B **46**, 15 887 (1992).